Chapter 3

Reduced magnetic braking and the magnetic capture model for the formation of ultra-compact binaries

M.V. van der Sluys, F. Verbunt and O.R. Pols

Abstract   A binary in which a slightly evolved star starts mass transfer to a neutron star can evolve towards ultra-short orbital periods under the influence of magnetic braking. This is called magnetic capture. In Chapter 2 we showed that ultra-short periods are only reached for an extremely small range of initial binary parameters, in particular orbital period and donor mass. Our conclusion was based on one specific choice for the law of magnetic braking, and for the loss of mass and angular momentum during mass transfer. In this chapter we show that for less efficient magnetic braking it is impossible to evolve to ultra-short periods, independent of the amount of mass and associated angular momentum lost from the binary.

3.1   Introduction

In Chapter 2 we examined the process of magnetic capture: a slightly evolved main-sequence star in a binary that transfers mass to a neutron-star companion while the orbital period shrinks to the ultra-short-period regime (less than about 40 minutes). To facilitate comparison with earlier work, we used the same law for magnetic braking, and the same assumption about the loss of mass and angular momentum during mass transfer as Podsiadlowski et al. (2002). Specifically, we used the law for magnetic braking as postulated by Verbunt & Zwaan (1981), with the extra requirement that a sufficiently large convective zone is present near the surface of the star, and we assumed that half of the transferred mass leaves the binary with the specific angular momentum of the neutron star. We concluded that ultra-short periods are reached within the Hubble time only by binaries within very narrow ranges of initial orbital periods and donor masses. In this chapter we investigate how this conclusion changes if we vary the assumptions on the strength of magnetic braking and on the loss of mass and angular momentum from the system.

Section 3.2 briefly describes the stellar evolution code used and especially the laws for magnetic braking and system mass loss that we implemented. We then show which grids of models were calculated and how the statistical study was performed in Sect. 3.3. The results are presented in Sect. 3.4 and discussed in Sect. 3.5. In Sect. 3.6 we summarise our conclusions.

3.2   Binary evolution code

3.2.1   The stellar evolution code

We calculate our models using the STARS binary stellar evolution code, originally developed by Eggleton (1971, 1972) and with updated input physics as described in Pols et al. (1995). Opacity tables are taken from OPAL (Iglesias et al. 1992), complemented with low-temperature opacities from Alexander & Ferguson (1994). For more details, see Sect. 2.2.

3.2.2   Angular momentum losses

Loss of angular momentum is essential to shrink the orbit of a binary in which the less massive star transfers mass to its more massive companion. We consider three sources of angular momentum loss.

For short periods, gravitational radiation is a strong source of angular momentum loss. We use the standard description

$$\frac{dJ_{\mathrm{GR}}}{dt} = -\frac{32}{5}\frac{G^{7/2}}{c^5}\frac{M_1^2\,M_2^2\,(M_1 + M_2)^{1/2}}{a^{7/2}} \tag{3.1}$$

(Peters 1984).

The second mechanism of angular momentum loss from the system is by non-conservative mass transfer. We assume that only a fraction β of the transferred mass is accreted by the neutron star. The remainder is lost from the system, carrying away a fraction α of the specific orbital angular momentum of the neutron star:

$$\frac{dJ_{\mathrm{ML}}}{dt} = -\alpha \,(1-\beta)\, a_1^2\, \omega\, \dot{M_2}, \tag{3.2}$$

where a_1 is the orbital radius of the neutron star and ω is the angular velocity.

To keep the models simple, we applied no regular stellar wind to our models, so that all mass loss from the system and associated angular momentum loss result from the non-conservative mass transfer described above.

The third source of angular momentum loss in this study is magnetic braking. Verbunt & Zwaan (1981) postulated a law for magnetic braking

$$\frac{dJ_{\mathrm{MB}}}{dt} = -3.8 \times 10^{-30}\, \eta\, M\, R^4\, \omega^3 \,\mathrm{dyn\,cm}, \tag{3.3}$$

on the basis of the observations by Skumanich (1972) that the equatorial rotation velocity v_e of main-sequence G stars decreases with the age t of the star as $v_e \propto t^{-0.5}$. In Chapter 2 we assumed $\eta = 1$, after Rappaport et al. (1983). More recent measurements of rotation velocities of stars in the Hyades and Pleiades, however, show that M stars have a wide range of rotation velocities that is preserved as they age (Terndrup et al. 2000). This indicates that magnetic braking is less strong for low mass stars than assumed in Eq. 3.3 with $\eta = 1$. Also, observational evidence indicates that coronal and chromospheric activity, and with it magnetic braking, saturate to a maximum level at rotation periods less than about 3 days (e.g. Vilhu 1982; Vilhu & Rucinski 1983). Verbunt (1984) showed that to explain a braking with the strength of Eq. 3.3 for a solar-type star, the star must have a magnetic field in excess of $\sim 200\,\mathrm{G}$ for a slow rotator, and in addition a stellar wind loss in excess of $5 \times 10^{-10} M_\odot$/yr for a fast rotator (for which the corotation velocity of the wind matter is much higher than the escape velocity – see also Mochnacki (1981)). A smaller field or less wind (for the fast rotator) automatically leads to a lower braking.

Many theoretical descriptions of angular momentum loss due to a magnetized wind can be found in the literature (among others Kawaler 1988; Stepien 1995; Eggleton & Kiseleva-Eggleton 2002; Ivanova & Taam 2003). These prescriptions depend on properties of the star (for instance wind mass loss rate, magnetic field strength, corona temperature) that are poorly known from observations for main-sequence stars and even less for evolving stars. These angular momentum prescriptions vary in strength and dependence on the stellar parameters. We have selected two different semi-empirical prescriptions to investigate the effect of reduced braking on the mechanism of magnetic capture. In Sect. 3.5 we will show that these two different implementations of magnetic braking dominate the evolution of the binary in two completely different phases of their life.

First, we retain the functional dependence of the braking on stellar mass and radius given by Eq. 3.3, but arbitrarily reduce the strength by taking $\eta = 0.25$ (reduced braking)

and $\eta = 0$ (no braking). Second, we use a new law for magnetic braking, derived on the basis of the ranges of rotation velocities in the Hyades and Pleiades, which includes saturation at a critical angular rotation velocity ω_{crit} (Sills et al. 2000):

$$\frac{dJ_{\mathrm{MB}}}{dt} = -K \left(\frac{R}{R_\odot}\right)^{0.5} \left(\frac{M}{M_\odot}\right)^{-0.5} \omega^3, \quad \omega \leq \omega_{\mathrm{crit}}$$

$$\frac{dJ_{\mathrm{MB}}}{dt} = -K \left(\frac{R}{R_\odot}\right)^{0.5} \left(\frac{M}{M_\odot}\right)^{-0.5} \omega\,\omega_{\mathrm{crit}}^2, \quad \omega > \omega_{\mathrm{crit}} \tag{3.4}$$

From Andronov et al. (2003) we take the value $K = 2.7 \times 10^{47}\,\mathrm{g\,cm^2\,s}$ that reproduces the angular velocity of the Sun at the age of the Sun. Krishnamurthi et al. (1997) require a mass-dependent value for ω_{crit} and they scale this quantity inversely with the turnover timescale for the convective envelope τ_{to} of the star at an age of 200 Myr:

$$\omega_{\mathrm{crit}} = \omega_{\mathrm{crit},\odot}\,\frac{\tau_{\mathrm{to},\odot}}{\tau_{\mathrm{to}}} \tag{3.5}$$

They use a fixed value for ω_{crit}, because they consider main-sequence stars and the value of τ_{to} does not change much during this evolution period. However, we consider donor stars in a binary system that change substantially during their evolution and hence use the instantaneous value for τ_{to}. This convective turnover timescale is determined by the evolution code by integrating the inverse velocity of convective cells, as given by the mixing-length theory (Böhm-Vitense 1958), over the radial extent of the convective envelope. We further use a value of $\omega_{\mathrm{crit},\odot} = 2.9 \times 10^{-5}\,\mathrm{Hz}$, equivalent to $P_{\mathrm{crit},\odot} = 2.5\,\mathrm{d}$ (Sills et al. 2000 find that a value for $\omega_{\mathrm{crit},\odot}$ of around 10 times the current solar angular velocity is needed to reproduce observational data of young clusters with a rigidly rotating model), and $\tau_{\mathrm{to},\odot} = 13.8\,\mathrm{d}$, the value that the evolution code gives for a $1.0\,M_\odot$ star at the age of 4.6 Gyr.

In both prescriptions (Eqs. 3.3 and 3.4) we follow Podsiadlowski et al. (2002) and reduce the magnetic braking by an ad hoc term

$$\exp(1 - 0.02/q_{\mathrm{conv}}) \quad \text{if } q_{\mathrm{conv}} < 0.02, \tag{3.6}$$

where q_{conv} is the fractional mass of the convective envelope. In this way we account for the fact that stars with a small or no convective mantle do not have a strong magnetic field and will therefore experience little or no magnetic braking. Notice that Eq. 3.5 alone predicts that stars with higher mass have a higher ω_{crit}, because they have a higher surface temperature, hence a smaller convective mantle and a shorter τ_{to}. The application of the term in Eq. 3.6 prevents that these stars experience unrealistically strong magnetic braking.

3.3 Creating theoretical period distributions

3.3.1 Binary models

Using the binary evolution code described in Sect. 3.2, with the non-saturated magnetic-braking law of Eq. 3.3 we calculated grids of models for Z=0.01, the metallicity of the

globular cluster NGC 6624, and Y=0.26. We choose initial masses between 0.7 and 1.5 $M_\odot$ with steps of 0.1 $M_\odot$. For each mass we calculated models with initial periods (P_i) between 0.5 and 2.5 days with steps of 0.5 d for all masses and dropped the lower limit for the initial period where necessary, down to 0.25 d. Around the bifurcation period between converging and diverging systems, where the shortest orbital periods occur, we narrow the steps in P_i to 0.05 or sometimes even 0.02 d.

Another series of models was calculated with a similar grid of initial masses and periods, but with the magnetic-braking law of Eq. 3.4 that includes saturation of the magnetic field strength at high angular velocities.

3.3.2 Statistics

In order to create a theoretical period distribution for a population of stars, we proceed as described in Sect. 2.4. First, we draw a random initial period (P_i) and calculate the time-period track for this P_i by interpolation from the two bracketing calculated tracks. Second, we pick a random moment in time and interpolate within the obtained time-period track to get the orbital period of the system at that moment in time. The system is accepted if mass transfer is occurring and the period derivative is negative. The details of this interpolation are described in Sect. 2.4.1. We do this 10^6 times for each mass to produce a theoretical orbital-period distribution for a given initial mass and given ranges in $\log P_i$ and time.

To simulate the period distribution for a population of stars with an initial mass distribution, we add the distributions of different masses. In Sect. 2.4.2 we show that the result depends very little on the weighting, so that we simulate a flat distribution in initial mass.

3.4 Results

3.4.1 Reduced magnetic braking

We have calculated three grids of models as described in Sect. 3.3.1 with the non-saturated magnetic-braking law given by Eq. 3.3. We have given the three grids different braking strengths by changing the value for η. We used the values $\eta = 1.0$ (as in Chapter 2), $\eta = 0.25$ and $\eta = 0.0$. For the last set, there is no magnetic braking and the angular momentum loss comes predominantly from gravitational radiation. For all models in these grids, half of the transferred mass is ejected from the system with the specific angular momentum of the neutron star, i.e. we used $\alpha = 1$ and $\beta = 0.5$ in Eq. 3.2. Figure 3.1 shows time-period tracks for models from the three grids with selected initial orbital periods and $M_i = 1.1\,M_\odot$.

The figure shows clearly that initially similar models evolve in different ways, but only after mass transfer has started. This is because a low-metallicity main-sequence 1.1 $M_\odot$ star has a high surface temperature, hence a small convective envelope ($q_{\mathrm{conv}} \approx 10^{-3}$) and therefore effectively no magnetic braking at that stage (see Eq. 3.6). After mass transfer starts, the surface temperatures drop and the differences in magnetic braking strength become apparent. It is obvious that a model that experiences weaker magnetic braking may
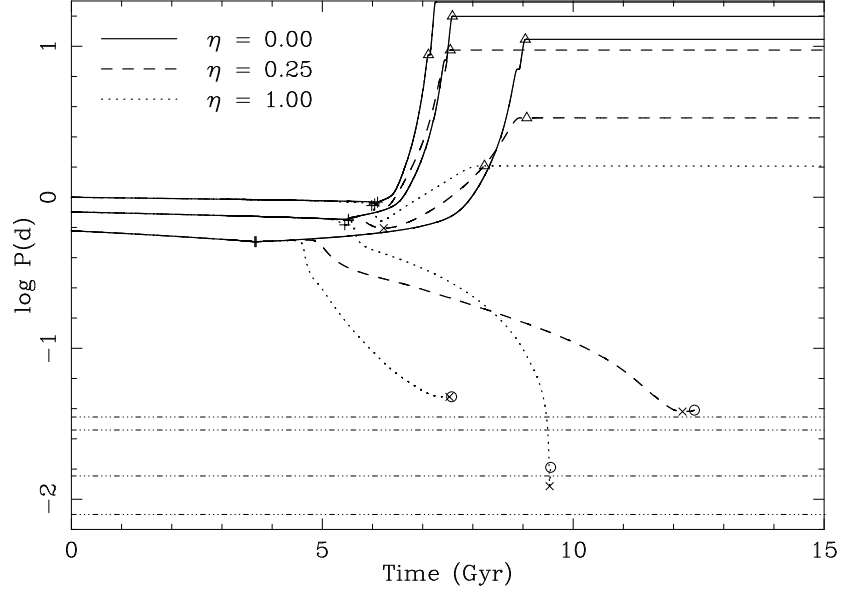
Figure 3.1: Time-period tracks for $Z = 0.01$, $M_i = 1.1 \, M_\odot$ with $P_i = 0.6 \, d$, $P_i = 0.8 \, d$, and $P_i = 1.0 \, d$. Each model is shown for three different values of η: 0.0 (solid lines), 0.25 (dashed lines) and 1.0 (dotted lines). The symbols mark special points in the evolution: $+$ marks the start of Roche-lobe overflow (RLOF), $\times$ the minimum period, $\triangle$ the end of RLOF and O marks the end of the calculation. The four dash-dotted horizontal lines show the orbital periods of the closest observed LMXBs in globular clusters: 11.4 and 20.6, and in the galactic disk: 41 and 50 minutes.

diverge where a similar model with stronger braking converges, and that models with weak magnetic braking converge slower than models with strong magnetic braking.

For each grid of models we produce a statistical sample as explained in Sect. 3.3.2. The results are period distributions for three populations of stars with initial masses between 0.7 and 1.5 $M_\odot$ and ages between 10 and 13 Gyr. The distributions are compared in Fig. 3.2.

The most striking difference in the period distributions for the three values of η is the shortest orbital period produced in the magnetic capture model. In models with reduced magnetic braking the orbits do not converge to ultra-short periods before the Hubble time, and the cut-off at the low-period end of the distribution accordingly lies at a higher period. This is also the reason why there are more systems with orbital periods of around 0.1 d for $\eta = 0.0$ than for $\eta = 1.0$; the missing models with stronger braking have already converged to lower orbital periods, or beyond the period minimum.
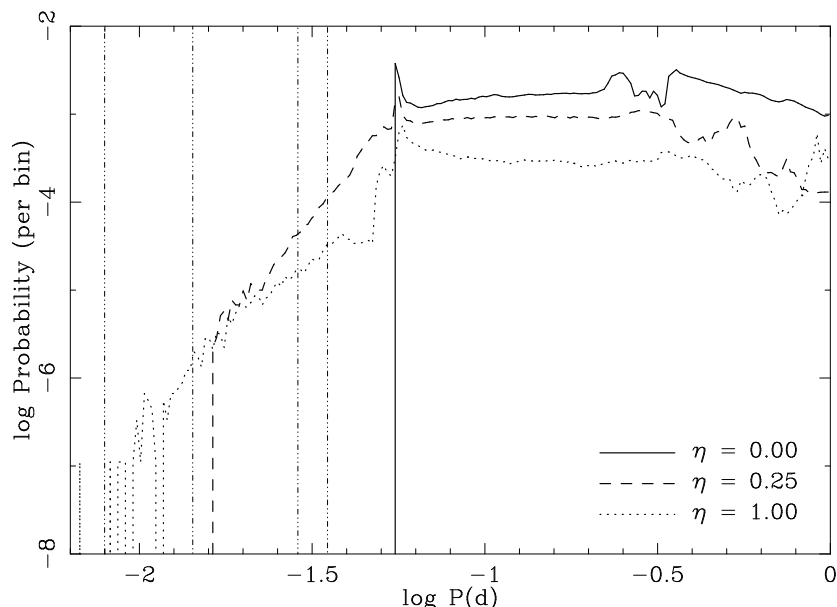
Figure 3.2: Period distributions for the magnetic capture model for $\eta = 0.0$ (solid lines), 0.25 (dashed lines) and 1.0 (dotted lines). It is clear that the cut-off for lower orbital periods strongly depends on the strength of the magnetic braking. The vertical axis displays the logarithm of the probability that an X-ray binary with a certain orbital period is found. The four vertical dash-dotted lines show the same observed orbital periods as the horizontal lines in Fig. 3.1. The probability is computed by distributing the accepted periods into bins of width $\Delta \log P = 0.011$ and dividing the number in each bin by the total number of systems.

3.4.2 Saturated magnetic braking

We have calculated one grid of models described in Sect. 3.3.1 with the saturated magnetic-braking law given by Eq. 3.4. In this prescription the magnetic field saturates at a certain critical angular velocity ω_{crit}, that depends on the convective turnover timescale of the donor star, as shown in Eq. 3.5. At an angular velocity higher than ω_{crit}, the magnetic braking scales linearly with ω rather than cubically. As the typical initial critical spin *period* is a few days, this is long compared to the initial orbital and – since the spins and orbits of our models are generally synchronised – spin period, and therefore replacing the prescription of Eq. 3.3 by that of Eq. 3.4 can be expected to have an effect similar to lowering the strength of the magnetic braking, as we did in Sect. 3.4.1. Because we will see in Sect. 3.4.3 that the shortest orbital periods are reached for models with conservative mass transfer, all models in this grid have $\beta = 1.0$ in Eq. 3.2.

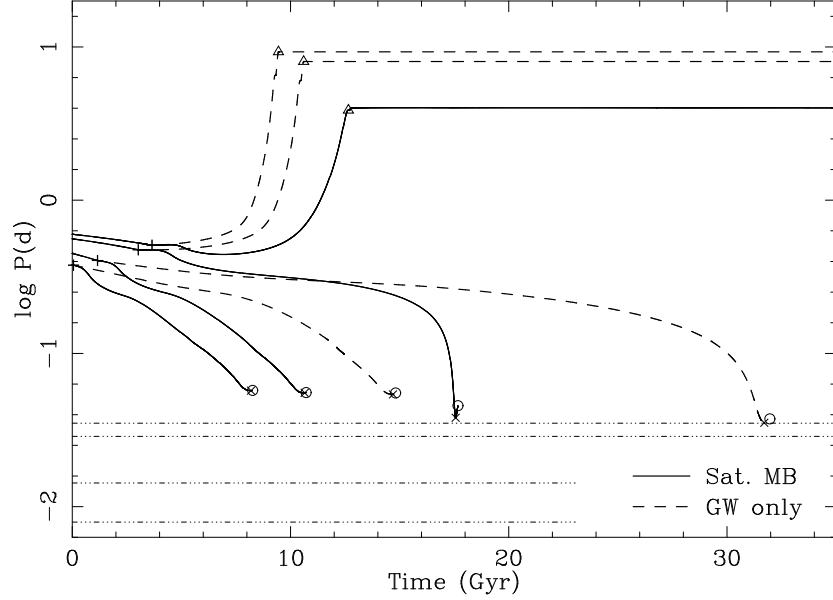Figure 3.3 compares the tracks of $1.1 M_{\odot}$ models from this grid with tracks taken from

Figure 3.3: Time-period tracks for $Z = 0.01$, $M_i = 1.1\,M_\odot$ with $P_i = 0.38\,d$ (the shortest possible P_i for this model), $P_i = 0.45\,d$, $P_i = 0.56\,d$, and $P_i = 0.60\,d$. Each model is shown for a magnetic braking law according to Eq. 3.4 (Sat. MB, solid lines) and no magnetic braking, but gravitational waves only (GW only, dashed lines). The symbols and horizontal dash-dotted lines are as in Fig. 3.1. Note that the time axis extends far beyond the Hubble time.

Sect. 3.4.3 with conservative mass transfer and without magnetic braking, i.e. $\beta = 1.0$ and $\eta = 0.0$. We see similar differences between the two sets of models as seen in Fig. 3.1, but the magnetic braking is clearly too weak to evolve the systems to less than 75 min within the Hubble time.

We performed statistics on the model as described in Sect. 3.3.2; the result is displayed in Fig. 3.4 and compared to the period distribution for a grid of models with $\beta = 1.0$ and $\eta = 0.0$.

3.4.3 The influence of mass loss

In Chapter 2 we have assumed that half of the transferred mass in our models is lost by the accretor and leaves the system with the specific angular momentum of the accretor. To see what influence this assumption has on the results of our study, we calculated a number of models with conservative mass transfer, so that $\beta = 1.0$ in Eq. 3.2. We calculated two sets of conservative models, one set without magnetic braking ($\eta = 0$ in Eq. 3.3) and one set with full braking ($\eta = 1$). The time-period tracks of selected models are compared to
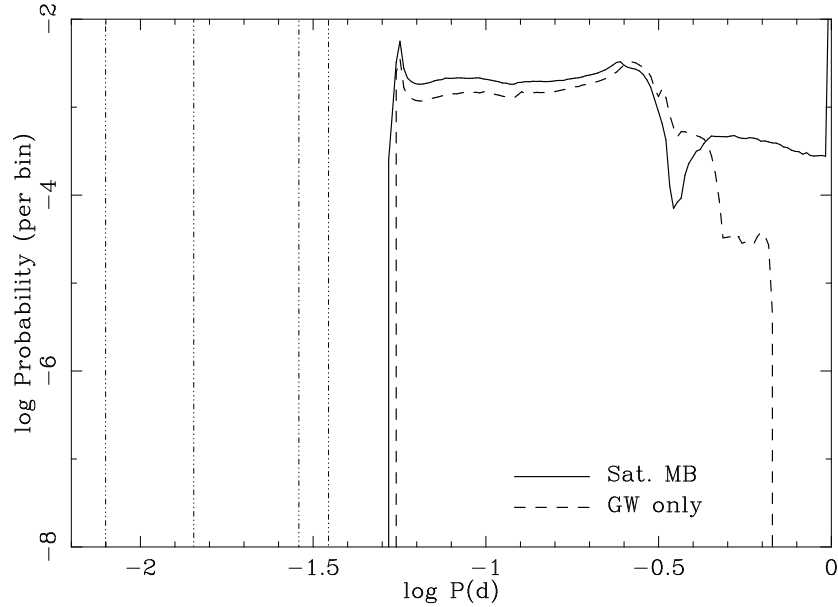
Figure 3.4: Period distribution for the magnetic capture model using the magnetic braking law described in Eq. 3.4 (Sat. MB, solid line) compared to the period distribution for models without braking, but with gravitational waves only (GW only, dashed line). The four vertical dash-dotted lines show the same observed orbital periods as the horizontal lines in Fig. 3.1. The probability is calculated in the same way as in Fig. 3.2.

previous models with $\beta = 0.5$ in Figs. 3.5 and 3.6.

Figure 3.5 shows that the time-period tracks of models with gravitational waves as the dominant angular momentum loss source are changed noticeably by a change in β. Converging models reach their minimum period much earlier for conservative models than for non-conservative models. The reason for this is that mass loss from the binary according to Eq. 3.2 leads to a widening of the binary for the value of α we use. However, even for the shortest possible initial period (0.38 d), and therefore the earliest possible period minimum for these systems, the time of the minimum shifts from 19.9 Gyr to 14.7 Gyr with a period of 78 min. The conclusion is that this effect makes no difference to the number or distribution of ultra-compact binaries.

For models with magnetic braking, the differences between the two sets of models is much smaller, as shown in Fig. 3.6. The reason for this is that the orbital evolution is completely dominated by the strong magnetic braking, so that changes in less important terms, like the amount of mass loss from the system and the associated angular momentum loss, are of very little influence. The models with full magnetic braking *can* produce ultra-compact binaries within the Hubble time; the distribution of ultra-short periods in these models is
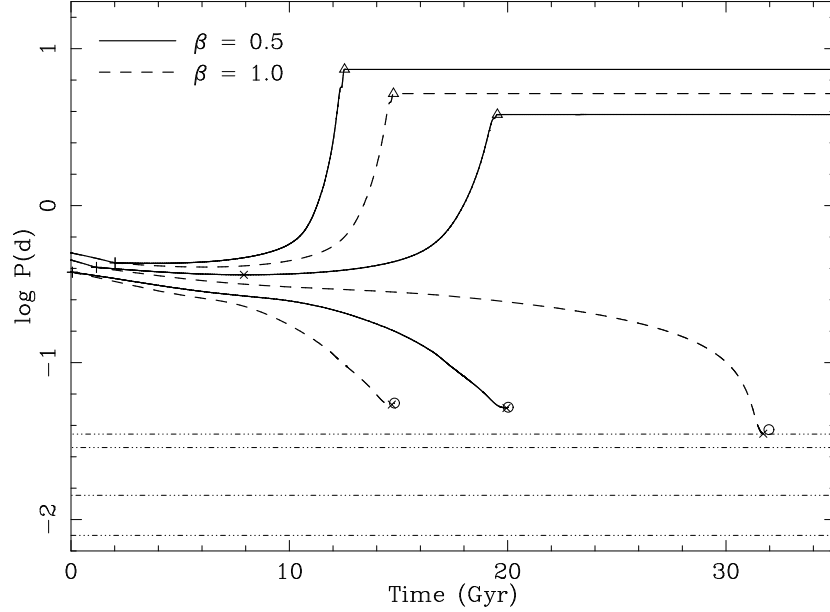
Figure 3.5: Time-period tracks for $Z = 0.01$, $M_i = 1.1\,M_\odot$ with $P_i = 0.38\,\text{d}$ (the shortest possible P_i), $P_i = 0.45\,\text{d}$ and $P_i = 0.50\,\text{d}$. Each model is shown for two different values of β ($\beta = 0.5$, solid lines and $\beta = 1.0$, dashed lines) and has no magnetic braking ($\eta = 0.0$). The symbols and horizontal dash-dotted lines are as in Fig. 3.1.

slightly affected by a change in β (see Fig. 3.6), but not enough to change the overall conclusion of Chapter 2.

3.5   Discussion

It is clear that the magnetic capture scenario to create ultra-compact binaries depends very strongly on the strength of the magnetic braking used. By simply scaling down the Verbunt & Zwaan (1981) prescription for magnetic braking, the results are, as can be expected intuitively,

- The bifurcation period between converging and diverging systems decreases, which means that only models with a lower initial orbital period will converge.

- The rate at which a system converges is lower, so that minimum periods are reached at a later time. This can imply that ultra-compact periods occur only after a Hubble time.
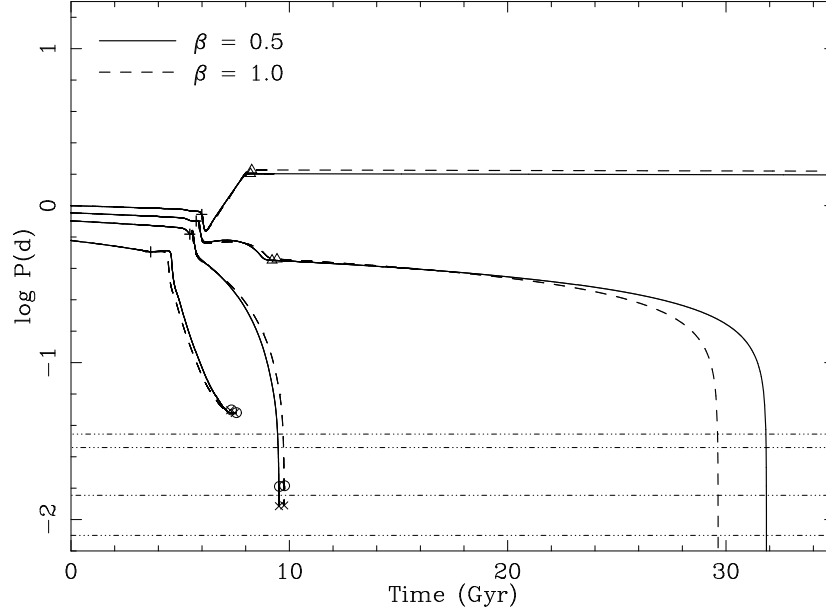
Figure 3.6: Time-period tracks for $Z = 0.01$, $M_i = 1.1 \, M_\odot$ with $P_i = 0.6 \, \text{d}$, $P_i = 0.8 \, \text{d}$, $P_i = 0.9 \, \text{d}$, and $P_i = 1.0 \, \text{d}$. Each model is shown for two different values of β ($\beta = 0.5$, solid lines and $\beta = 1.0$, dashed lines) and has full magnetic braking ($\eta = 1.0$). The symbols and horizontal dash-dotted lines are as in Fig. 3.1.

- Because reaching the minimum period takes much longer, a small offset in the initial period has much more impact on the evolution of the system. Because of this, the initial period range that leads to ultra-compact systems for a certain initial mass is much smaller and thus the chances of actually producing an ultra-compact system decrease.

If we use a slightly more sophisticated, saturated magnetic braking law, the results are qualitatively similar to decreasing the magnetic braking strength. Because of the different dependencies of the two different magnetic braking laws on the mass and radius of the star in Eqs. 3.3 and 3.4, the two prescriptions take effect at completely different parts of the evolution. To illustrate this, we picked three models with an initial mass of $1 \, M_\odot$ that evolve to the same minimum period (28 min) at about the same mass (0.06–0.07 $M_\odot$). The three models have different magnetic braking laws implemented and are given different initial periods to reach the desired P_{min}: the first model uses braking according to Eq. 3.3 and $P_i = 1.485 \, \text{d}$ so that the period minimum is reached after 11.7 Gyr. The second model loses angular momentum according to the saturated magnetic braking law in Eq. 3.4. It has $P_i = 1.109 \, \text{d}$ and needs 20.1 Gyr. The third model has no magnetic braking but only gravitational waves to lose angular momentum. It needs the shortest initial period (0.4998 d)

and longest evolution time (42 Gyr) to reach the desired minimum period.

The three models are compared in Fig. 3.7. The data are shown as a function of the total mass of the donor, starting with the onset of Roche-lobe overflow. Fig. 3.7a displays the orbital evolution of the three models. Due to loss of angular momentum, the orbital periods at the start of mass transfer are already significantly shorter than the periods P_i at the ZAMS. The model with the magnetic braking law of Eq. 3.3 has the longest orbital period at the onset of RLOF, but shrinks fast and coincides with the model without magnetic braking in the end. The dashed line of the model with the saturated magnetic braking from Eq. 3.4 intersects the solid line twice before the period minimum, indicating that braking starts out weaker, but ends stronger than the canonical magnetic braking of Eq. 3.3. This is clearly seen in Fig. 3.7b, where for each model two competing time scales are plotted: the time scale in which the mass transfer from the less massive to the more massive component would expand the orbit if it were the only process going on, and the timescale in which angular momentum loss (the sum of gravitational radiation and magnetic braking) would shrink the orbit if nothing else would happen. In order to obtain the timescale at which the orbital period changes (τ_P) due to angular momentum loss ($\dot{J}$), we use the fact that the total angular momentum of a binary scales with the cubed root of the orbital period ($J_{\mathrm{orb}} \propto P_{\mathrm{orb}}^{1/3}$) and thus

$$\tau_P = \frac{P_{\mathrm{orb}}}{\dot{P}_{\mathrm{orb}}} = \frac{P_{\mathrm{orb}}}{\frac{dP}{dJ}\dot{J}_{\mathrm{orb}}} = \frac{J_{\mathrm{orb}}}{3\dot{J}_{\mathrm{orb}}}. \tag{3.7}$$

To calculate τ_P due to angular momentum loss we substitute for $\dot{J}_{\mathrm{orb}}$ in Eq. 3.7 the sum of the angular momentum losses due to gravitational radiation and magnetic braking. The period derivative due to conservative mass transfer from star 1 to star 2, assuming no angular momentum loss, is given by:

$$\dot{P}_{\mathrm{orb}} = 3P_{\mathrm{orb}}\frac{M_1 - M_2}{M_1 M_2}\dot{M}_1 \tag{3.8}$$

which can be substituted into Eq. 3.7 to get τ_P. Depending on which of the two timescales is shorter, the orbit will expand or shrink. At the period minimum, the two lines for each model intersect. The figure shows that the timescales for the model with the canonical magnetic braking and the model with gravitational radiation only coincide around the period minimum. This happens because at these short orbital periods the models with canonical braking have very weak magnetic braking due to their small masses and radii (see Eq. 3.3) and therefore gravitational wave emission dominates the orbital evolution. It can be clearly seen in the figure that the timescales for the model with saturated magnetic braking are almost two orders of magnitude shorter than for the two other models and the orbital evolution is driven by the strong magnetic braking. Figure 3.7c shows the true period derivatives of the three models, which could have been inferred from the difference between the lines in Fig. 3.7b. It shows clearly that the orbit changes fastest for the model with canonical magnetic braking in the first part of the evolution, but faster for the model with the saturated magnetic braking law when the donor mass drops below about $0.2\,M_\odot$. Interestingly, the

model with saturated magnetic braking is in the saturated regime during all of the evolution, so that the difference in strength comes from the different dependence on the mass and radius of the donor. The deep dips in Fig. 3.7c are the period minima where $\dot{P}$ changes sign. Figure 3.7 illustrates that the two magnetic braking prescriptions that we use work at completely different phases of the evolution of the model. The canonical braking model of Eq. 3.3 acts mainly in the first part of the mass transfer phase, well before the period minimum, up to the point where the orbital period has decreased enough for gravitational radiation to take over as the main angular momentum loss mechanism and evolve the orbit to the ultra-short period regime. The saturated magnetic braking prescription of Eq. 3.4 is only slightly stronger than the gravitational radiation in the first part of the evolution, but becomes orders of magnitude stronger at shorter orbital periods and evolves to the ultra-compact binary state without any significant contribution in the angular momentum loss from gravitational radiation. Despite these large differences, there is little influence on the outcome of our statistical study. We therefore conclude that our study is independent of the the details of the magnetic braking, and that the use of other theoretical or semi-empirical laws mentioned in Sect. 3.2 will lead to similar results.

3.6 Conclusions

In Chapter 2 we showed that for magnetic braking according to Verbunt & Zwaan (1981) the formation of ultra-short-period binaries via magnetic capture is possible, albeit very improbable, within the Hubble time. In this chapter we find that for less strong magnetic braking, in better agreement with recent observations of single stars, the formation of ultra-short-period binaries via magnetic capture is even less efficient. Specifically, for magnetic braking reduced to 25% of the standard prescription (according to Eq. 3.3), the shortest possible period is 23 min; for saturated magnetic braking (according to Eq. 3.4) the shortest possible period is essentially the same as without magnetic braking, about 70 min.

Loss of mass and associated angular momentum from the binary in general widens the orbit and thereby delays the formation of ultra-compact binaries. However, this effect is only noticeable in the absence of magnetic braking.

An attractive feature of the magnetic capture model is its ability to explain the negative period derivative of the 11-minute binary in the globular cluster NGC 6624 (Van der Klis et al. 1993b; Chou & Grindlay 2001). Since we find that for a more realistic magnetic braking law it is impossible to create ultra-compact binaries via magnetic capture at all, it becomes less likely that the negative period derivative is intrinsic. Van der Klis et al. (1993a) show that an apparent negative period derivative can be the result of acceleration of the binary in the cluster potential. According to measurements with the HST the projected position of the binary is very close to the cluster centre, which makes a significant contribution of gravitational acceleration to the observed period derivative more likely (King et al. 1993).
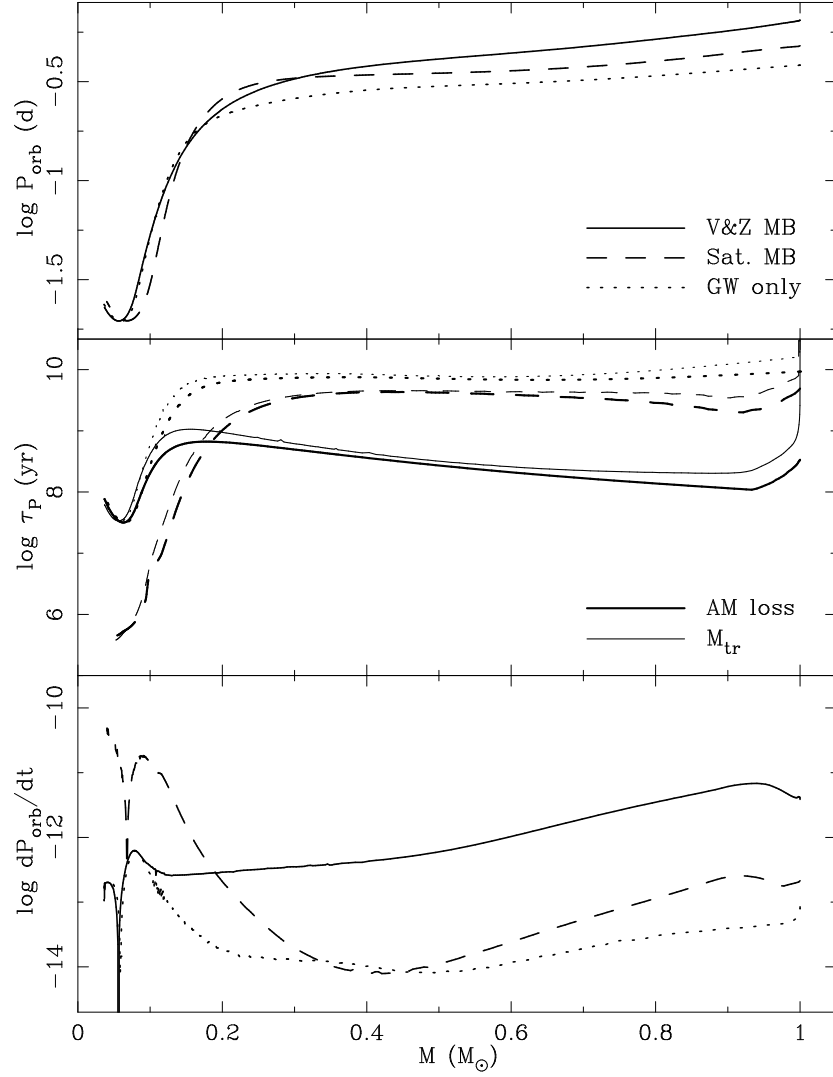
Figure 3.7: *Upper panel* (**a**): The logarithm of the orbital period. The line styles show the different models: with magnetic braking according to Eq. 3.3 (V&Z MB, solid line), with magnetic braking according to Eq. 3.4 (Sat. MB, dashed line) and without magnetic braking (GW only, dotted line). *Middle panel* (**b**): The logarithm of the timescales of orbital shrinkage due to angular momentum loss (AM loss, thick lines) and orbital expansion due to the mass transfer (M_{tr}, thin lines). The line styles represent the different models as in (a). *Lower panel* (**c**): The logarithm of (the absolute value of) the orbital period derivative in dimensionless units. The line styles are as in (a).